Naval Research Laboratory
Stennis Space Center, MS 39529-5004

NRL/MR/7322--95-7684

Variations of Ice Cover and Thermohaline Structure in the Arctic-GIN Sea Basin: Analysis of Model Results for the 1986–1990 Period

RICHARD A. ALLARD
STEVE A. PIACSEK

Ocean Dynamics and Prediction Branch
Oceanography Division

January 26, 1996

DISCLAIMER NOTICE

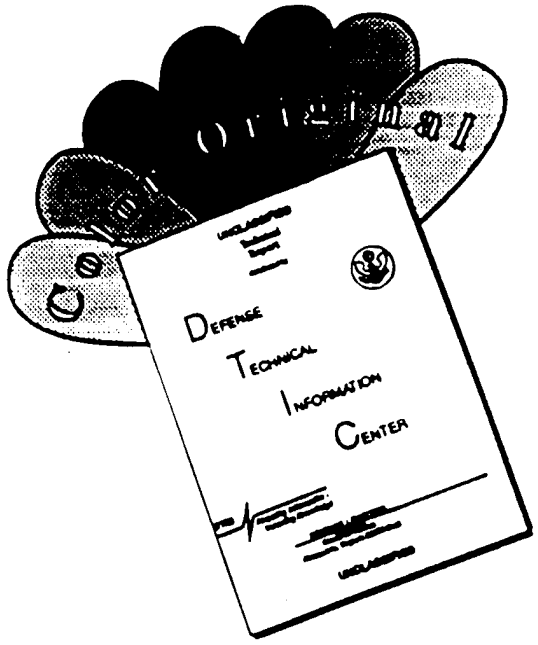

THIS DOCUMENT IS BEST QUALITY AVAILABLE. THE COPY FURNISHED TO DTIC CONTAINED A SIGNIFICANT NUMBER OF COLOR PAGES WHICH DO NOT REPRODUCE LEGIBLY ON BLACK AND WHITE MICROFICHE.

REPORT DOCUMENTATION PAGE

Form Approved
OBM No. 0704-0188

1. AGENCY USE ONLY *(Leave blank)*	2. REPORT DATE	3. REPORT TYPE AND DATES COVERED
	January 26, 1996	Final

4. TITLE AND SUBTITLE

Variations of Ice Cover and Thermohaline Structure in the Arctic-GIN Sea Basin: Analysis of Model Results for the 1986–1990 Period

5. FUNDING NUMBERS

Job Order No. 573505405
Program Element No. DOE
Project No.
Task No. ER61733
Accession No. DN154008

6. AUTHOR(S)

Richard A. Allard and Steve A. Piacsek

7. PERFORMING ORGANIZATION NAME(S) AND ADDRESS(ES)

Naval Research Laboratory
Oceanography Division
Stennis Space Center, MS 39529-5004

8. PERFORMING ORGANIZATION REPORT NUMBER

NRL/MR/7322--95-7684

9. SPONSORING/MONITORING AGENCY NAME(S) AND ADDRESS(ES)

U.S. Department of Energy
D.C. Bader, Sp. Rep. (CHAMMP Director)
Washington, D.C. 20585

10. SPONSORING/MONITORING AGENCY REPORT NUMBER

11. SUPPLEMENTARY NOTES

12a. DISTRIBUTION/AVAILABILITY STATEMENT

Approved for public release; distribution unlimited.

12b. DISTRIBUTION CODE

13. ABSTRACT *(Maximum 200 words)*

Thermodynamic changes in the Arctic ice cover and ocean have been investigated for the years 1986–1990 with a coupled ice-ocean numerical model. The model basin includes the Barents and GIN (Greenland-Iceland-Norwegian) Seas on a polar stereographic grid with 127 km resolution. The coupled model consists of the Hibler ice model, a 3-D advective turbulent mixed layer model based on the Mellor-Yamada level 2.5 closure scheme, and a diagnostic inverse model for the geostrophic currents. The pressure gradients for the geostrophic flow are derived from the Levitus climatology, as are the influxes of heat and salt at the open boundaries. The atmospheric momentum and heat fluxes were derived from 6-hourly Navy Operational Global Atmospheric Prediction System (NOGAPS) output for the years 1986–1990.

Analysis has focused on interannual variations of the total ice volume, ice edge position and ice circulation, the thermohaline structure, and the turbulent energy associated with the inertial-Ekman currents available for mixing. These variations have been computed for the whole model domain, as well as in the Arctic Basin proper, the GIN Sea and the Greenland Sea (the MIZEX zone).

The range of interannual variations for the ice cover is found to be much greater in the summer than in the winter, with magnitudes up to 50% and 10% of the mean seasonal variation. The summer minima of the total ice volume and ice covered area form a half period of an oscillating cycle: 1986 and 1990 having minima of about the same strength and 1988 a maximum. There is a negative correlation between these cycles and the annual wind strengths, which have maxima in the years 1986 and 1990.

The thermohaline structure of the surface layers is found to undergo marked changes beginning in the fall of 1988. The GIN Sea has acquired a cold bias of about .20°C between October 1988 and March 1989, thereafter following the usual seasonal variations. The Central Arctic, on the other hand, has experienced a warming trend in the same period, leading to a warming of about .0075°C. In somewhat of a contrast, the annual mean salinities in both the GIN Sea and the Central Arctic have increased monotonically throughout the 5 years. Only after June of 1990 does the salinity in the Central Arctic decline to the 1988 fall values.

14. SUBJECT TERMS	15. NUMBER OF PAGES
coupled ice-ocean model, ocean/climate models, sea ice analysis	40
	16. PRICE CODE

17. SECURITY CLASSIFICATION OF REPORT	18. SECURITY CLASSIFICATION OF THIS PAGE	19. SECURITY CLASSIFICATION OF ABSTRACT	20. LIMITATION OF ABSTRACT
Unclassified	Unclassified	Unclassified	SAR

Variations of Ice Cover and Thermohaline Structure in the Arctic-GIN Sea Basin: Analysis of Model Results for the 1986-1990 Period

Richard Allard and Steve Piacsek

Naval Research Laboratory

Stennis Space Center, MS, 39529

October, 1995

Abstract

Thermodynamic changes in the Arctic ice cover and ocean have been investigated for the years 1986-1990 with a coupled ice-ocean numerical model. The model basin includes the Barents and GIN (Greenland- Iceland-Norwegian) Seas on a polar stereographic grid with 127 km resolution. The coupled model consists of the Hibler ice model, a 3-D advective turbulent mixed layer model based on the Mellor-Yamada level 2.5 closure scheme, and a diagnostic inverse model for the geostrophic currents. The pressure gradients for the geostrophic flow are derived from the Levitus climatology, as are the influxes of heat and salt at the open boundaries. The atmospheric

momentum and heat fluxes were derived from 6-hourly Navy Operational Global Atmospheric Prediction System (NOGAPS) output for the years 1986-1990.

Analysis has focussed on interannual variations of the total ice volume, ice edge position and ice circulation, the thermohaline structure, and the turbulent energy associated with the inertial-Ekman currents available for mixing. These variations have been computed for the whole model domain, as well as in the Arctic Basin proper, the GIN Sea and the Greenland Sea (the MIZEX zone).

The range of interannual variations for the ice cover is found to be much greater in the summer than in the winter, with magnitudes up to 50% and 10% of the mean seasonal variation. The summer minima of the total ice volume and ice covered area form a half period of an oscillating cycle: 1986 and 1990 having minima of about the same strength and 1988 a maximum. There is a negative correlation between these cycles and the annual wind strengths, which have maxima in the years 1986 and 1990.

The thermohaline structure of the surface layers is found to undergo marked changes beginning in the fall of 1988. The GIN Sea has acquired a cold bias of about $.20°C$ between October 1988 and March 1989, thereafter following the usual seasonal variations. The Central Arctic, on the other hand, has experienced a warming trend in the same period, leading to a warming of about $.0075°C$. In somewhat of a contrast, the annual mean salinities in both the GIN Sea and the Central Arctic have increased monotonicly throughout the five years. Only after June of 1990 does the salinity in the Central Arctic decline to the 1988 fall values.

1 Introduction

An interesting question concerning climate change is the response of the Arctic ice pack to global warming. Many research studies have focussed recently on the seasonal and interannual variations of the Arctic ice cover, comprising both observational data analyses and model simulations. Some of the observational studies were performed by Walsh and Johnson (1979), Parkinson *et al.* (1987) and Rothrock and Thomas (1990). Parkinson *et al.* (1987) have studied microwave observations of the Arctic ice cover for the years 1973-1976, and most recently Gloersen *et al.* (1994) analyzed Arctic (and Antarctic) sea ice for the period 1978-1987, and found a large interannual variability.

Earlier modeling works have examined the seasonal and multi-year variations in the ice cover using ice-only models [Parkinson and Kellogg (1979), Hibler and Walsh (1982), Walsh *et al.* (1985)]. More recent studies have utilized coupled ice-ocean models. The seasonal variation for 1986 has been investigated by Piacsek *et al.* (1991), and for 1986 and 1989 by Riedlinger and Preller (1991). The seasonal and interannual variations for the years 1971-1980 has been studied by Fleming and Semtner (1991) who have studied the effect of interannually varying ocean currents on the ten-year evolution of ice, and have found a significant impact on the interannual variations. Most of these studies have used interannually varying mean monthly winds and heat fluxes for surface forcing, the exceptions being Piacsek *et al.* (1991) and Riedlinger and Preller (1991), who have employed daily synoptic forcing derived from GCM output.

It is to be expected, and was in fact explicitly or implicitly assumed in all the above studies, that the annual variations of the ice cover and underlying water masses will reflect

the seasonal and annual variations in the forcings. These forcings include the overlying atmospheric momentum and heat fluxes, and fluxes associated with ocean currents entering the domain from the North Atlantic and Pacific Oceans, through the Greenland-Iceland-United Kingdom (GIUK) Gap and the Bering Strait, respectively.

Unfortunately, at the moment very few data are available on the inflow transports for the last five years or so. Thus we have decided to concentrate our present studies, concerned with simulating the ice cover for the five-year period 1986-1990, on the effects of the atmospheric forcings, allowing only a mean seasonal variation for these transports. Since we have used atmospheric forcing from operational GCM outputs, i.e. from models that perform daily assimilation of observed pressures and temperatures [both remotely sensed and in-situ], we expect a certain degree of realistic correlation between the interannual changes in the atmosphere and those computed for Arctic ice cover and the underlying thermohaline structure.

2 Description of the Model

The coupled ice-ocean model used in these interannual studies has been described in detail in Piacsek *et al.* (1991) and Warn-Varnas *et al.* (1991). The model contains essentially three components: the Hibler (1979) ice model, and a 3-D ocean model that consists of a turbulent mixed layer model and an inverse geostrophic model. Coupling between the three models is achieved as follows: the ice is coupled to the ocean through flux boundary conditions (including heat, salt and momentum); the mixed layer, in turn, is coupled one-way to a climatological background ocean, receiving advection velocities from

a geostrophic inverse model. There is no direct feedback from the computed temperature and salinity changes to the geostrophic currents, i.e. pressure is determined solely from the seasonally evolving, predetermined climatological density field. The computed Ekman drift and Ekman divergence, however, also contribute horizontal and vertical advection velocities, respectively, to the mixed layer model. On the thermodynamic side, the ocean model calculates the mixed layer temperature, freezing temperature, and oceanic heat flux for the ice model, while the ice model determines the stress between the ice and the water, and the salinity flux under the ice cover. The Hibler ice code was modified to utilize the mixed layer temperatures, freezing temperatures, and oceanic heat fluxes calculated in the ocean model. The heat budget routine includes the seven level thickness distribution after Walsh *et al.* (1985).

On the momentum side, the ocean contributes a velocity to the ice-water drag that is the sum of the inertial, Ekman, and geostrophic velocities. In turn, the ice momentum equations furnish ice velocities that enter into the ice-water drag force. Since a full turbulent mixed layer model is used, we employ the ice-water drag rather than the modified wind stress (wind stress minus internal ice stress) as the upper boundary conditions on the ocean [Svensson and Omstedt (1990)]. In open water regions the atmospheric fluxes are used directly for the upper boundary conditions. If a grid cell is ice-covered, the wind stress and the heat fluxes are applied to the ice first, and then the ice-water drag is computed to drive the ocean.

Some additional model particulars will now be described. To simulate the evolution of the mixed layer under the ice, and in general the thermodynamic changes in the ocean, we utilize the TOPS (Thermodynamic Ocean Prediction System) model that has been

operational at FNMOC (Fleet Numerical Meteorological and Oceanography Command) in Monterey, CA for several years [Clancy and Pollak (1983)]. For this study, the model has been modified to extend to the ocean bottom. The TOPS model employs the Mellor and Yamada (1974) Level-2.5 turbulence closure method to parameterize the vertical eddy fluxes of temperature, salinity and momentum.

A weak three-year relaxation is imposed on the the temperature and salinity fields below 50m to prevent the solutions from straying too far from climatology on long model integrations. Our tests with lower or zero values of this constant produced no significant differences in either ice thickness or concentration, and none on the synoptic or monthly time scales [see also Hibler and Bryan (1987)]. The geostrophic velocity at all levels of the ocean is calculated with a beta-spiral type inverse method of Peggion (1988), utilizing seasonal varying density fields derived from the Levitus (1982) climatological temperature and salinity fields. The model assumes the usual hydrostatic and geostrophic approximations, and additional constraints are imposed on the density field due to mass conservation and the topography [see Olbers *et al.* (1985)]. The resulting linear equations fitting all constraints to the data are solved through a minimization procedure. The computed geostrophic currents are then interpolated to monthly values.

The barotropic (i.e. vertically averaged) current is composed of two parts: a wind-driven part obtained from a simple one-layer shallow water model, and a part obtained from the inverse model which includes the J-bar effect of the topography-stratification interaction. The horizontal density gradients were found to be very weak in the Arctic, so that north of the Iceland-Faeroe Front the wind (and inflow) forcings completely dominate the barotropic flow. The climatological wind effects are contained in the density field, and

the synoptic response is adequately represented by the one-layer model.

The entire coupled ice-ocean model is defined at equal grid intervals of 127 km on a polar stereographic projection, with a total horizontal resolution of 47x25 grid points (Figure 1). The vertical grids of the TOPS and the inverse models coincide, containing 17 levels in a stretched configuration, with a resolution that places 9 points in the first 100 meters and varies from $5m$ near the surface to several hundred meters near the bottom. The resolution is designed to track variations in the mixed layer, rather than track variations of the bottom topography. This grid also corresponds to the grid used by the PIPS (Polar Ice Prediction System) of the Navy in a daily operational setting [Preller (1985)]. In summary, the ice and the upper ocean are represented prognostically, and the interior ocean diagnostically.

3 Model Initialization and Forcing

The temperature and salinity fields in the ocean model are initialized from the Levitus(1982) winter climatology, with the values below 1500m depth blended with the Levitus annual climatology. The ice cover is initialized by specifying a uniform ice cover of 3 meters everywhere in the model domain, and setting the ice velocities to zero. By the second year of simulation, the ice cover closely resembles the final distribution.

The model is forced by 6-hourly atmospheric fluxes derived from the NOGAPS model of FNMOC, for the year 1986-1990. The model was extensively tested for year 1986 by Piacsek *et al.* (1991) and Riedlinger and Preller (1991), because in 1986 good quality ice concentration and buoy velocity observations were available to check the model results.

The reason for using 6-hourly forcing is two-fold: (a) the inclusion of an active, turbulent, prognostic mixed layer model requires the use of daily, and preferably 6-hourly, momentum and heat fluxes; (b) the spatial resolution of the GCM forcing is twice that of the climatology, i.e. 2.5x2.5 degrees rather than the 5x5 degrees of Walsh *et al.* (1985). A further argument in favor of the GCM fluxes is the consistency between momentum and the evaporative and sensible heat fluxes, since they are all derived from a model in which they played an integral role to begin with.

Somewhat contrary results were found by Hibler and Bryan (1987), who investigated the effect on ice drift and thickness distribution due to differences in the climatological and 1979 FGGE forcing. They have found a great improvement in the ice thickness distribution and the ice drift patterns using the climatological winds. On the other hand, the studies using 6-hourly GCM forcing reported in Piacsek *et al.* (1991) and Riedlinger and Preller (1991) all have demonstrated even much better ice thickness distributions, ice edge positions and comparison with buoy drifts. At any rate, to look at interannual variations this was found to be the easiest, if not the best, approach.

The first 8 months of 1988 the GCM atmospheric fluxes were of inferior quality and had to be omitted; instead the average of the four other years was used to supply a continuity of forcing. This was expected to yield reduced wind stresses, mixing energy and ice velocities, and as we shall see subsequently, this was indeed the case. On the one hand, this led to an interruption of the continuous 6-hourly forcing; on the other hand, it led to an interesting illustration of the differences obtained in the ice cover and water mass structure when using climatological and daily surface forcing. It also yielded an insight into the thermodynamic and dynamic inertia associated with the ice and the upper 200m

of the ocean.

In open water regions these fluxes are used directly for the upper boundary conditions for temperature and salinity, and wind stress for momentum. If a grid cell is ice-covered, the wind stress and the heat fluxes is applied to the ice first, and then the ice-water drag is computed to drive the ocean. With the exception of the salt flux, which is specified if the presence of an ice cover, precipitation and evaporation are assumed to be zero for our model calculations.

4 Model Results and Analysis

4.1 Variation of Atmospheric Fluxes

In order to interpret the model results for the annual variations of the ice cover and the underlying water masses, we will examine briefly the annual variations in the forcings: the surface air temperature, and the momentum and heat fluxes.

Figure 2 and Figure 3 show the variation of the surface air temperature during the five years of our model simulation, 1986-1990, for the Arctic Basin proper and the Greenland Sea, respectively. The bold contours in each figure show the 5-year average surface air temperature, indicating that there is some interannual variability whose significance we will try to establish in these studies. In the Greenland Sea region, the colder than "normal" winters of 1989 and 1990 are indicated by the relatively cold temperatures during the January-March period of 1989, and in 1990 an even longer cold period persists through the end of May. There is less variation during the summer months, because there is usually an upper limit to which the Greenland Sea air temperatures can rise due to increased cloud

cover. In the Arctic basin proper, the warm episode in the Chukchi and Beaufort Seas in 1990 is illustrated to some degree by the relatively warmer temperatures for the first half of 1990.

4.2 Variations of the Ice Cover

As the first quantitative estimate of these variations, we have computed the total area covered with ice for which the concentration exceeds 15 percent, and the corresponding ice volume. Figure 4 displays the time history of the total ice volume and total ice covered area contained in our model domain, from January 1986 to December 1990. We see that the range of the interannual variations for the winter is only about 10 percent of the mean seasonal change, but about 50 percent in the summer. The five summer minima represent the half period of a cycle, with the 1986 and 1990 summers having minima of equal strengths and 1988 having a maximum. In agreement with earlier results, summer ice extent is a sensitive indicator of surface air temperature changes in the Arctic.

We may recall that in 1988 we had to use climatological winds and heat fluxes (averaged over the other four years) as forcing for the first 8 months of the year, and this could very well be the cause of the high summer ice volume in 1988. We shall see below (in Tables 1 through 4) that the kinetic energy of the inertial/Ekman currents in the upper 200m also displays a cyclic behavior, with maxima in 1986 and 1990, and a minimum in 1988. Since these energies are directly correlated with wind strength, it would appear then that the summer ice extent is somehow correlated with the annual wind strength for that particular year. The air temperatures (Figures 2 and 3) and the heat fluxes (not shown) don't seem to contain anything resembling this cycle in their interannual behav-

ior. Perhaps, a more sensitive indicator of the interannual variations, we display the 0.5m and 2.5m thickness contours in Figures 5a and 5b for the five winters and summers, respectively. For clarity, we must mention that winter here means January-March and summer July-September. We can see in Figure 5a that in the Greenland Sea, the ice edge had its furthest extent in 1990, while it is a minimum in 1987. In the Barents Sea, where the weak model-generated barotropic currents keep the ice edge too far south [Piacsek *et al.* (1991)], there is little variation in the ice edge except for 1989, when it has its maximum extent. We also display the 2.5 m contours to illustrate ice growth patterns in the Arctic basin proper. The thickest ice (not shown), in excess of 4 meters, is found near the Canadian Archipelago, in agreement with observations. We can see that the years 1989 and 1990, in addition to showing the greatest southward extent, also have thicker ice near the pole that extends toward Spitsbergen and the Greenland Sea. In the summer, the situation is similar, with the 1990 ice edge having the furthest extent in the Barents and Greenland Seas, while it has retreated to its most northerly position in 1987.

It must be pointed out, of course, that ice extent or ice edge position by itself is only a qualitative indication of total ice volume and oceanic area covered. This would explain some of the discrepancies between the results of Figure 4 and the ice edge positions shown in Figures 5a and 5b. There are unfortunately no direct ice thickness measurements available to check the volume simulations for the years 1986-1990, though there are some earlier results available [Bourke and Garrett (1987)]. Recent microwave techniques have been able to distinguish between old and young ice. With the old ice being generally thicker, these measurements can hopefully shed light on total ice present, but still only in a semi-quantitative way.

4.3 Variation in Water Mass Structure

Results were computed for each of the four regions depicted in Figure 1: the Arctic-GIN Sea domain, the GIN Sea, the Greenland Sea (MIZEX area), and the Arctic Basin. In one approach, we have plotted the seasonal variations of the mean temperature and salinity for each of the five years in two regions: the GIN Sea (Figures 6 and 7) and the Central Arctic (Figures 8 and 9), respectively. In these figures the temperatures and salinities have been averaged over all depths and grid points falling within the respective regions, with a further averaging over all time steps falling within a day. In another approach, we have plotted the seasonal evolution of the depth of selected isotherms and isohalines for each of the five years in the Greenland Sea (Figures 10 and 11). In the Central Arctic, the displacements were found to be too small for a meaningful analysis. Finally, we have displayed in detail the vertical dependence of these variations (including that of the mixing energy) in Tables 1-4 for each of the four regions. Here the mean temperatures and salinities have been computed across four layers whose depths and thicknesses correspond roughly to 0-20m, 20-100m, 100-200m, and 200-800m, respectively.

4.3.1 Interannual changes in the seasonal variation

A joint examination of Figures 6-11 and Tables 1-4 reveals that the thermohaline structure has undergone marked changes, beginning in the fall of 1988, and with opposite trends in the GIN Sea and Central Arctic. In the GIN Sea (Table 2), the surface(0-20m) layer has acquired a cold bias of about $.9°C$ (based on the difference between the 1986-88 and 1989-1990 means), and the 20-100m layer a bias of about $.35°C$. During this period, the mean temperature of the whole volume cooled about $.05°C$, thereafter following the

usual seasonal variation for the rest of 1989 and throughout 1990. An examination of the 5 year mean versus climatology (column 6 of Table 2) shows the largest deviation from climatology to occur at depth: whereas the surface (0-20m) layer has a cold bias of .70^{o}C, the 20-100m and 100-200m layers have biases of 1.44 and 1.81 ^{o}C, respectively.

In the Central Arctic (Table 4), on the other hand, a warming trend has set in at the end of October 1988 (Figure 8), leading to a warm bias of about .0075^{o}C throughout the volume. In the surface layer, this warming is much more pronounced: in the top (0-20) layer it's about .05^{o}C, but below that (down to 800m) it's about .01^{o}C on the average. After March 1989, the temperature resumes its normal seasonal variation. In this region the deviations from climatology show a cold bias of .35^{o}C in the surface layer, and .21 and .09 ^{o}C in the 20-100m and 100-200m layers, respectively.

The corresponding annual salinity variations are displayed in Figures 7 and 9. In each year, one can see the basic trend toward higher salinities during the fall and winter months when ice is growing, and toward lower salinities during the spring and summer months when ice is melting. However, the interannual variations show a different behavior from that of the temperature. In the GIN Sea, salinity increases throughout the volume in the fall of 1988 and 1989, and also in March of both 1989 and 1990 (Figure 7). Thus 1989 and 1990 have the highest mean salinities, with successive increases of about .0005 *ppt*, respectively. In fact, Table 2 shows that in all layers between 0-200m the salinity has increased monotonicly from 1986 to 1990, with 1989 and 1990 being .045 and .085 *ppt* saltier in the surface (0-20m) layer than the 1986-1988 period, respectively. The corresponding increases in the 20-100m layer were about .025 and .055 *ppt*, respectively. As was the case with the temperature, the 1986-1988 curves tended to cluster into a

group, and the 1989 and 1990 curves were then offset from the first group and then 1989, respectively, by biases of about .0005 *ppt*. This very small figure is however for the deep volume average; the surface changes (between 0 and 200m) ranged between .025 to .085 *ppt*. A comparison of the 5 year mean versus climatology shows a salt bias of +.01 *ppt* in the surface layer, but freshness biases of .03 *ppt* in the 20-100m layer and .08 *ppt* in the 100-200m layer.

In somewhat of a contrast, the salinity changes expressed different trends with depth in the Central Arctic. Figure 9 shows that the (volume-averaged) winter-spring mean of the salinity has increased monotonicly throughout the 1986-1990 simulation period. The July-August values for 1988, 1989 and 1990 are about the same, but substantially higher than the 1986 and 1987 values. 988 values. The annual growth in the salinity bias is about .003 *ppt* for the volume-mean. The same mean annual increase is found in the 20-100m layer, as shown in Table 4. However, the surface layer exhibits a different behavior: the salinity increases from 32.24 in 1986 to 32.53 in 1988; thereafter it declines to 32.50 in 1989 and 32.45 in 1990. Comparison of the 5 year mean with the climatology (column 6 of Table 4) shows some drastic departures in the upper layers: the surface layer (0-20m) is saltier by 1.69 *ppt*, the 20-100m layer by .76 *ppt*, and the 100-200m layer by .005 *ppt*.

In summary, we will point out that in the GIN Sea, the seasonal variations of both T and S fall into three groups. The first group consists of the 1986- 1988 curves that follow each other closely. The second and third group each consists of one year, 1989 and 1990, respectively, whose curves are offset by roughly the same cold bias and salinity increase from the first group and from 1989, respectively (Figures 7 and 9), making 1990 the coldest and saltiest year in our study. One noteworthy result is that the 5 year mean

is about $.7°C$ colder than climatology, but only .01 *ppt* saltier.

4.3.2 Depth of isotherms and isohalines

Another useful way of illustrating changes in the T-S structure, particularly any cooling or warming trends, is to plot the depth of given isotherms and isohalines as a function of time. Figure 10 displays the depth-time behavior of the .25 (and .50 $°C$ isotherm for each of the five years. The qualitative behavior with seasons is very similar for all the years, but the actual depths attained show a division into two groups. The years 1986-1988 follow each other fairly closely, but the years 1989 and 1990 form a loose group with much greater depths. For all years from the beginning of January to the end of March, during the coldest period, the isotherm keeps descending to a minimum which is a strong function of the year: for 1986-1988 this hovers about a depth of $200 - 250m$, whereas in 1989 and 1990 this depth was found to be below 450m. Then the isotherm begins its ascent due to spring/summer warming, but while this rise terminates at the end of June for the first group, it continues into September for 1989 and 1990. We note that starting in the April/May period, a second isotherm of .25 $°C$ appears at the surface, which then descends to meet the rising companion at about the 125m depth. Interestingly, this depth is the same for all years. The only exception is the year 1990, in which the isotherms never meet, signifying the persistence of colder water throughout the year in the depth range 100-200m. Near the end of November, the isotherm commences its descent due to surface cooling.

Similarly, the depth of the 34.6 *ppt* isohaline is illustrated in Figure 11. The principal factor affecting salinity in the upper ocean, besides advection, is the surface salinity flux,

with brine rejection due to winter freezing, and fresh water formation due to summer melting. As was the case with the .25 $^{\circ}C$ isotherm, the five isohalines divide into two distinct groups. The isohalines of 1986-1988 follow each other quite closely, whereas the isohalines of 1989-1990 follow each other at considerably shallower depths, indicating a general 'saltification' of the upper 100 m during these years. At the end of 1988 the isohaline begins to shallow at a much steeper rate than in the previous years, so instead of leveling off at 50m, it rises to about 20m. It then repeats the previous years' cycle, except that it remains flat from mid-March to mid-May, i.e. remains at about the 20m depth. The year 1990, starting with the 1989 'bias', also repeats the usual summer/fall cycle. It exhibits, however, peculiar peaks in February and May. It appears that when the isohaline is so shallow, it can be exposed more easily to the synoptic storms' mixing, bringing them closer to the surface.

4.4 Discussion

There are several interesting and/or peculiar aspects of the simulation results that warrant an explanation, or at least some physical understanding. Regarding the ice cover, the first two interesting observations made concerning Figure 4 are: the winter ice volumes and ice covered areas have a small interannual variation, but the summer values have a large one. Two factors that bear on this and are likely to have significant interannual variations, namely wind strength and air/water temperatures, are evidently much more effective when the ice is thin and more disbursed than when it is thick and compacted. The strong inverse correlation between wind strength ($\tilde{U}$ in Table 1) and summer ice volume supports this: years 1986 and 1990 have the largest Ekman layer velocities and

also the smallest summer ice volumes . The strong winds can accomplish this in two or three ways: (1) they can move ice from cold, dense regions (e.g. from the Central Basin to the Greenland Sea) to warmer regions near marginal zones where melting is more likely to take place through stronger atmospheric heating and/or contact with warmer ocean currents, or (2) they can increase vertical mixing which can bring up warmer water to be in contact with the ice. Concerning the winter values, this correlation appears to be weak but definitely present for total ice volume. However, it fails for 1986, as well as for the ice covered area values. Correlation with air temperatures (Figures 2 and 3) is more difficult to establish. The unusually cold winter of 1986 in the Arctic Basin could explain the above normal winter ice volume in that year. Similarly, the winter and spring were unusually warm in 1987 in the Greenland Sea, and in 1989 in the Central Arctic, and that could account for the small winter ice volumes associated with those years. On the other hand, the unusually cold winters of 1989 and 1990 did not seem to effect total ice volume (but as we have seen, they do affect ocean temperature and ice extent very much).

It is interesting to note that the maximum southward extent of ice in the the summers of 1989 and 1990 in the Greenland Sea (Figure 3) is accompanied by the least southward extent in the Beaufort and Chukchi Seas, with the net result that those years have small amounts of total ice in the summer. Since air temperatures in the GIN Sea (Figure 3) are colder than normal in the summer of 1989 and about average in 1990, we have a partial explanation for the Greenland Sea but not for the Arctic, where the summer temperatures in these years are normal.

5 Conclusions

The results of this report show that it is possible to simulate interannual variations of the ice cover and thermohaline structure in the Arctic-GIN Sea Basin using GCM-derived forcing fluxes and an advective oceanic mixed layer. In general, total ice volume and ice covered area in a given year depends on the total wind energy of that year. The summer extent of ice depends on both the air temperature and the oceanic temperature and salinity associated with the respective marginal ice zone. The surface salinity increases monotonicly from 1986 to 1990, whereas the ocean surface peaks in 1987 and then declines monotonicly. For the whole basin, the ocean is much colder and much more salty than the corresponding Levitus climatology for each of the five simulation years.

6 Acknowledgments

The authors would like to thank Shelley Riedlinger of NRL for many stimulating discussions concerning details of the FNMOC forcing fluxes. This work was performed as part of the Naval Research Laboratory's 6.1 Ice Modeling project, PE 0601153N. Partial support of the Department of Energy's CHAMMP Program (Grant DE-AI05-93ER61733) is acknowledged. Computing was performed on the Cray YMP at CEWES of the US Army in Vicksburg, MS., as part of the HPCI program of the DOD.

7 References

Aagaard, K., E. C. Carmack, The role of sea ice and other fresh water in the Arctic circulation. J. Geophys. Res. 94, 14485-14498, 1989.

Bourke, R. H. and R. P. Garrett, Sea ice thickness distribution in the Arctic Ocean, Cold Regions Science and Technology 13, 259-280, 1987.

Clancy, R. M. and K. D. Pollak, A real-time synoptic ocean thermal analysis/forecast system, Prog. Oceanogr. 12, 383-424, 1983.

Hibler, W. D.,III., and K. Bryan, A diagnostic ice-ocean model, J. Phys. Oceanogr. 17, 987-1015, 1987.

Hibler, W. D., III, A dynamic thermodynamic sea ice model, J. Phys. Oceanogr., 9, 815-846, 1979.

Levitus, S., Climatological Atlas of the World Ocean. NOAA Professional Paper 13, 173 pp, 1982.

Manabe, S. ,R. J. Stouffer,M. J. Spelman, and K. Bryan, Transient Response of a coupled ocean-atmosphere model to gradual changes of atmospheric CO2. Part 1:annual mean response. J. of Climate 4, p.785, 1991.

Martin, P. J., Simulation of the mixed layer at OWS November and Papa with several models, J. Geophys. R., 90, 903, 1985.

Mellor, G. L., and T. Yamada, A hierarchy of turbulence closure models for planetary boundary layers. J. Atmos. Sci., 31, 1791-1806, 1974.

Olbers, D. J., M. Wenzel, and J. Willebrand, The inference of North Atlantic circulation patterns from climatological hydrographic data. Rev. of Geophys. 23, 313-356,

1985.

Parkinson, C. L., C. J. Josefino, H. J. Zwally, D. J. Cavalieri, P. Gloersen and W. J. Campbell, Arctic Sea Ice 1973:1976: Satellite Passive Microwave Observations. NASA SP-489, National Aeronautics and Space Administration, Washington,D.C. 296 pp.

Parkinson, C. L. and W. M. Washington, A large-scale numerical model of sea ice, J. Geophys. Res., 84, 311-337, 1979.

Parkinson, C. L. and W.M.Kellogg, Arctic sea ice decay simulated for a CO2-induced temperature rise. Climatic Change 2, p.149, 1979.

Peggion, G., A Method for Determining Absolute Velocities from Hydrographic Data. SACLANT Research Centre Report SR-114, 28 pp., 1987.

Piacsek, S. A., R. Allard and A. Warn-Varnas, Studies of the Arctic Ice Cover With a Coupled Ice-Ocean Model. J. Geophys. Res. 96, 4631-4650., 1991.

Preller, R. H., The NORDA/FNOC Polar Ice Prediction system (PIPS)- Arctic: A Technical Description. NORDA Tech. Report 108, Naval Research Laboratory, Stennis Space Center, MS, 60 pp, May 1985.

Riedlinger, S. and R. H. Preller, The Development of a Coupled Ice-Ocean Model for Forecasting Ice Conditions in the Arctic. J. Geophys. Res. 96, p.16955, 1991.

Semtner, A. J. Jr., A model for the thermodynamic growth of sea ice in numerical investigations of climate. J. Phys. Oceanogr. 6, 379-389, 1976.

Semtner, A. J. Jr., A numerical study of sea ice and ocean circulation in the Arctic. J. Phys. Oceanogr. 17, 1077, 1987.

Walsh, J. E., W. Hibler III, and B. Ross, Numerical simulation of northern hemisphere sea ice variability, 1951-1980. Jour. Geophys. R., 90, 4847-4865, 1985.

Warn-Varnas,A. R. Allard and S. Piacsek, Synoptic and seasonal variations of the ice-ocean circulation in the Arctic: a numerical study. Annals of Glaciol. 15, p.54, 1991.

8 Table Captions

Table 1. Layer-averaged profiles of T, S, and speed of the inertial-Ekman motions $|U|$ (cm/sec),computed for the whole Arctic/GIN Sea domain.

Table 2. Layer-averaged profiles of T, S, and speed of the inertial-Ekman motions $|U|$ (cm/sec), computed for the GIN Sea area (grid I=28,46; J=2,15 of Figure 1).

Table 3. Layer-averaged profiles of T, S, and speed of the inertial-Ekman motions $|U|$ (cm/sec), computed for the Greenland Sea area (grid I=28,37; J=2,12 of Figure 1).

Table 4. Layer-averaged profiles of T, S, and speed of the inertial-Ekman motions $|U|$ (cm/sec), computed for the Arctic Basin (grid I=2,26; J=2,28 of Figure 1).

9 Figure Captions

Figure 1. (a) Map of the combined Arctic-Greenland Sea Basin, showing the employed computational domain and grid. The area referred to as the GIN Sea is the box bounded by X=28,46 and Y=2,15; the Greenland Sea area is the box bounded by X=28,37 and Y=2,12; and the Arctic Basin is denoted by X=2,26 and Y=2,28.

Figure 2. Seasonal and interannual variation of the surface air temperature in the Arctic basin proper.

Figure 3. Seasonal and interannual variation of the surface air temperature in the Greenland Sea area.

Figure 4. Seasonal and interannual evolution of the total ice volume (a) and ice covered area (b) over the whole Arctic/GIN Sea domain.

Figure 5a. Ice thickness contours for the years 1986-1990 in the winter season (January-March). The ice edge is represented by the .5m contour lines; the 2.5m contour depicts roughly the beginning of the thick-ice areas.

Figure 5b. Same as 5a, except for the summer season (July-September).

Figure 6. The seasonal evolution of the mean temperature in the GIN Sea area for each of the five year span 1986-1990.

Figure 7. The seasonal evolution of the mean salinity in the GIN Sea area for each of the five year span 1986-1990.

Figure 8. The seasonal evolution of the mean temperature in the Arctic Basin for each of the five year span 1986-1990.

Figure 9. The seasonal evolution of the mean salinity in the Arctic Basin for each of

the five year span 1986-1990.

Figure 10. Seasonal evolution of the depth of the .25 $^{\circ}C$ isotherm in the GIN Sea for each of the five years 1986-1990.

Figure 11. Seasonal evolution of the depth of the 34.6 *ppt* isohaline in the GIN Sea for each of the five years 1986-1990.

T A B L E 1

LAYER-AVERAGED PROFILES OF T,S,|U|

FOR COMPLETE ARCTIC/GIN SEA DOMAIN

MEAN T(Z)

DEPTH	TV86	TV87	TV88	TV89	TV90	TVLV
0 - 20 m	0.08	0.10	-0.08	-0.15	-0.16	0.78
20 - 100 m	-0.30	-0.26	-0.39	-0.40	-0.51	0.55
100 - 200 m	-0.12	-0.09	-0.09	-0.17	-0.25	0.68
200 - 800 m	0.76	0.78	0.80	0.75	0.71	1.06

MEAN S(Z)

DEPTH	SV86	SV87	SV88	SV89	SV90	SVLV
0 - 20 m	33.06	33.18	33.25	33.24	33.23	32.05
20 - 100 m	33.47	33.49	33.54	33.54	33.58	33.03
100 - 200 m	33.98	33.98	33.99	33.99	34.00	34.02
200 - 800 m	34.68	34.68	34.68	34.68	34.68	34.70

MEAN U(Z)

DEPTH	UV86	UV87	UV88	UV89	UV90
0 - 20 m	32.14	26.64	15.50	26.41	32.39
20 - 100 m	6.08	4.16	2.62	5.40	5.97
100 - 200 m	0.12	0.08	0.07	0.32	0.31
200 - 800 m	0.01	0.00	0.00	0.02	0.03

T A B L E 2

DEPTH-AVERAGED PROFILES OF T,S,|U|

FOR THE GIN SEA AREA

MEAN T(Z)

DEPTH	TV86	TV87	TV88	TV89	TV90	TVLV
0 - 20 m	4.16	4.40	3.94	3.28	3.12	4.48
20 - 100 m	2.92	3.11	2.75	2.59	2.21	4.16
100 - 200 m	2.12	2.20	2.26	1.96	1.72	3.86
200 - 800 m	2.04	2.09	2.12	1.95	1.85	2.52

MEAN S(Z)

DEPTH	SV86	SV87	SV88	SV89	SV90	SVLV
0 - 20 m	34.61	34.64	34.65	34.68	34.72	34.65
20 - 100 m	34.77	34.77	34.78	34.80	34.83	34.82
100 - 200 m	34.89	34.89	34.89	34.89	34.90	34.97
200 - 800 m	35.01	35.01	35.02	35.01	35.01	35.04

MEAN U(Z)

DEPTH	UV86	UV87	UV88	UV89	UV90
0 - 20 m	50.76	36.42	20.07	43.17	43.35
20 - 100 m	10.94	7.22	4.61	9.47	9.57
100 - 200 m	0.22	0.18	0.19	0.64	0.77
200 - 800 m	0.01	0.01	0.01	0.06	0.11

T A B L E 3

DEPTH-AVERAGED PROFILES OF T,S,|U|

FOR THE GREENLAND SEA

MEAN T(Z)

DEPTH (m)	TV86	TV87	TV88	TV89	TV90	TVLV
0 - 20	1.09	1.36	0.71	0.26	0.22	1.20
20 - 100	0.15	0.32	-0.06	-0.11	-0.32	0.87
100 - 200	-0.16	-0.10	-0.12	-0.30	-0.42	0.89
200 - 800	0.23	0.26	0.27	0.04	-0.02	0.72

MEAN S(Z)

DEPTH (m)	SV86	SV87	SV88	SV89	SV90	SVLV
0 - 20	34.15	34.22	34.25	34.32	34.34	34.19
20 - 100	34.45	34.45	34.47	34.52	34.54	34.48
100 - 200	34.65	34.67	34.67	34.68	34.69	34.75
200 - 800	34.90	34.90	34.91	34.90	34.90	34.93

MEAN U(Z)

DEPTH (m)	UV86	UV87	UV88	UV89	UV90
0 - 20	52.16	32.10	19.09	41.77	43.31
20 - 100	11.20	6.49	4.36	8.76	9.44
100 - 200	0.24	0.16	0.19	0.64	0.75
200 - 800	0.01	0.01	0.01	0.06	0.09

T A B L E 4

DEPTH-AVERAGED PROFILES OF T,S,|U|

FOR THE ARCTIC BASIN

MEAN T(Z)

DEPTH	TV86	TV87	TV88	TV89	TV90	TVLV
0 - 20	-1.64	-1.69	-1.72	-1.63	-1.54	-1.29
20 - 100	-1.63	-1.65	-1.68	-1.66	-1.65	-1.44
100 - 200	-1.26	-1.26	-1.28	-1.27	-1.27	-1.18
200 - 800	0.07	0.09	0.10	0.12	0.11	0.07

MEAN S(Z)

DEPTH	SV86	SV87	SV88	SV89	SV90	SVLV
0 - 20	32.24	32.46	32.53	32.50	32.45	30.75
20 - 100	32.76	32.80	32.85	32.86	32.89	32.07
100 - 200	33.44	33.44	33.44	33.45	33.46	33.44
200 - 800	34.51	34.51	34.51	34.51	34.51	34.52

MEAN U(Z)

DEPTH	UV86	UV87	UV88	UV89	UV90
0 - 20	16.69	15.16	9.07	15.69	23.17
20 - 100	1.18	1.62	0.74	1.66	2.71
100 - 200	0.01	0.01	0.00	0.01	0.02
200 - 800	0.00	0.00	0.00	0.00	0.00

COUPLED ICE/OCEAN MODEL GRID
RESOLUTION 127 X 127 KM

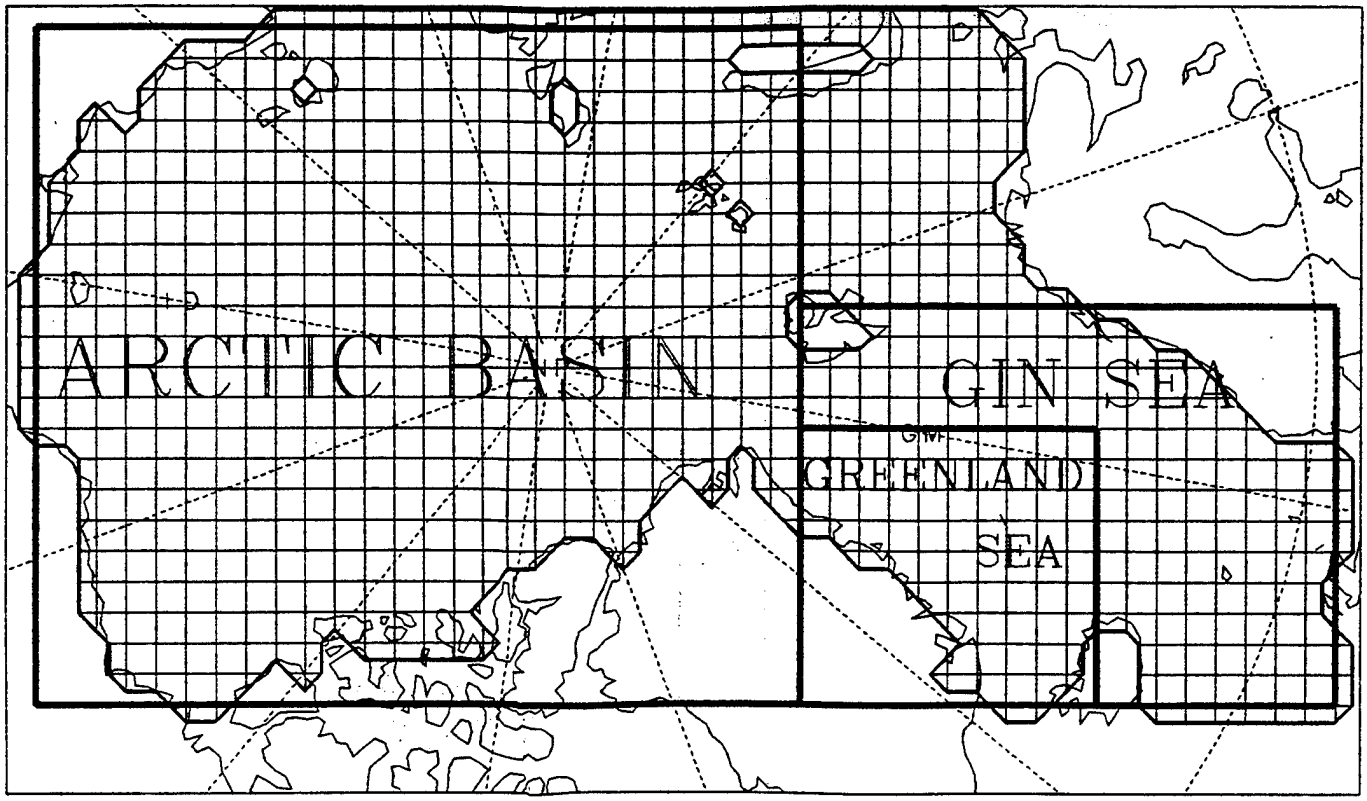

Fig. 1

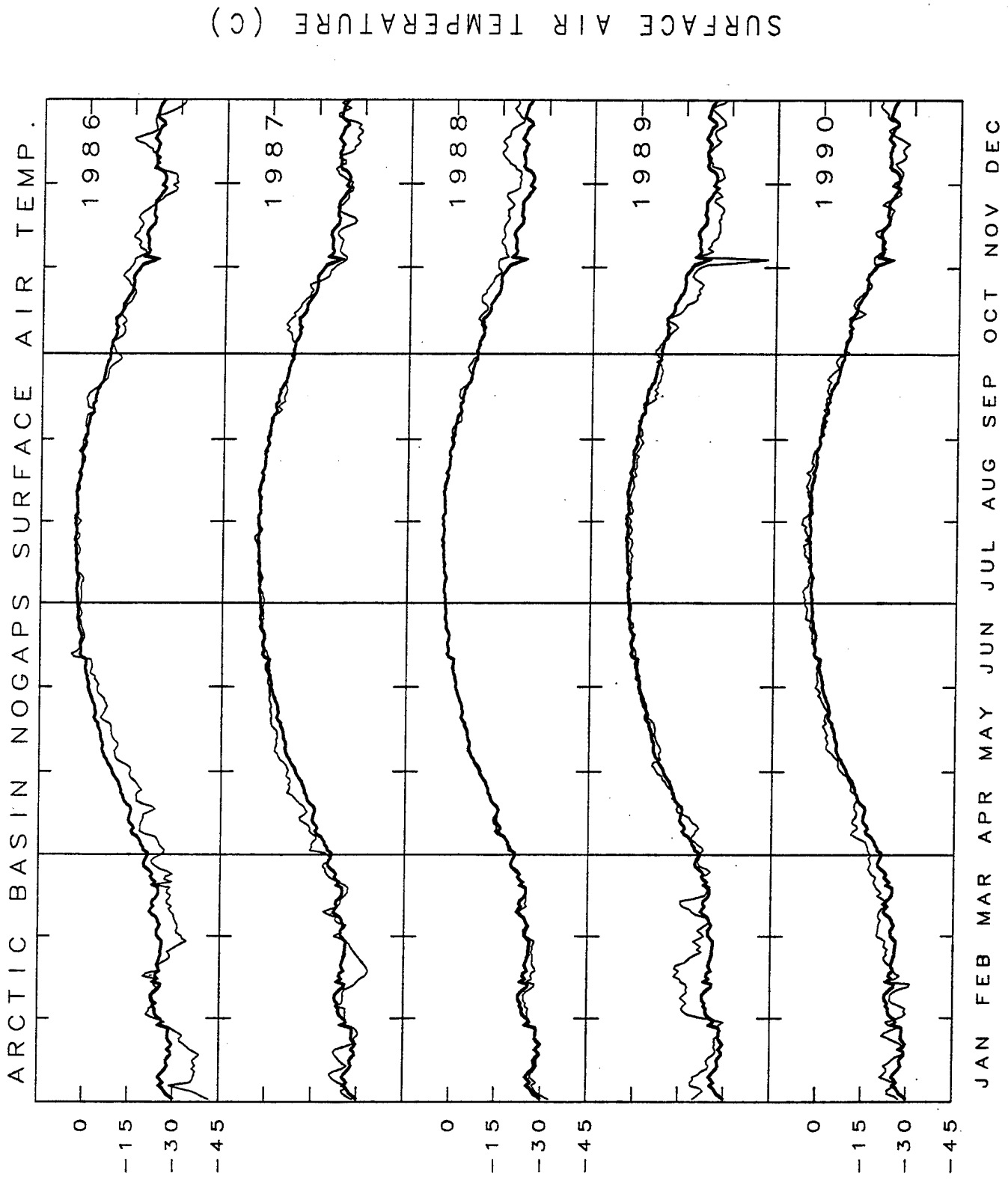
SURFACE AIR TEMPERATURE (C)
ARCTIC BASIN NOGAPS SURFACE AIR TEMP.
1986
1987
1988
1989
1990
0
-15
-30
-45
JAN FEB MAR APR MAY JUN JUL AUG SEP OCT NOV DEC

Fig. 2

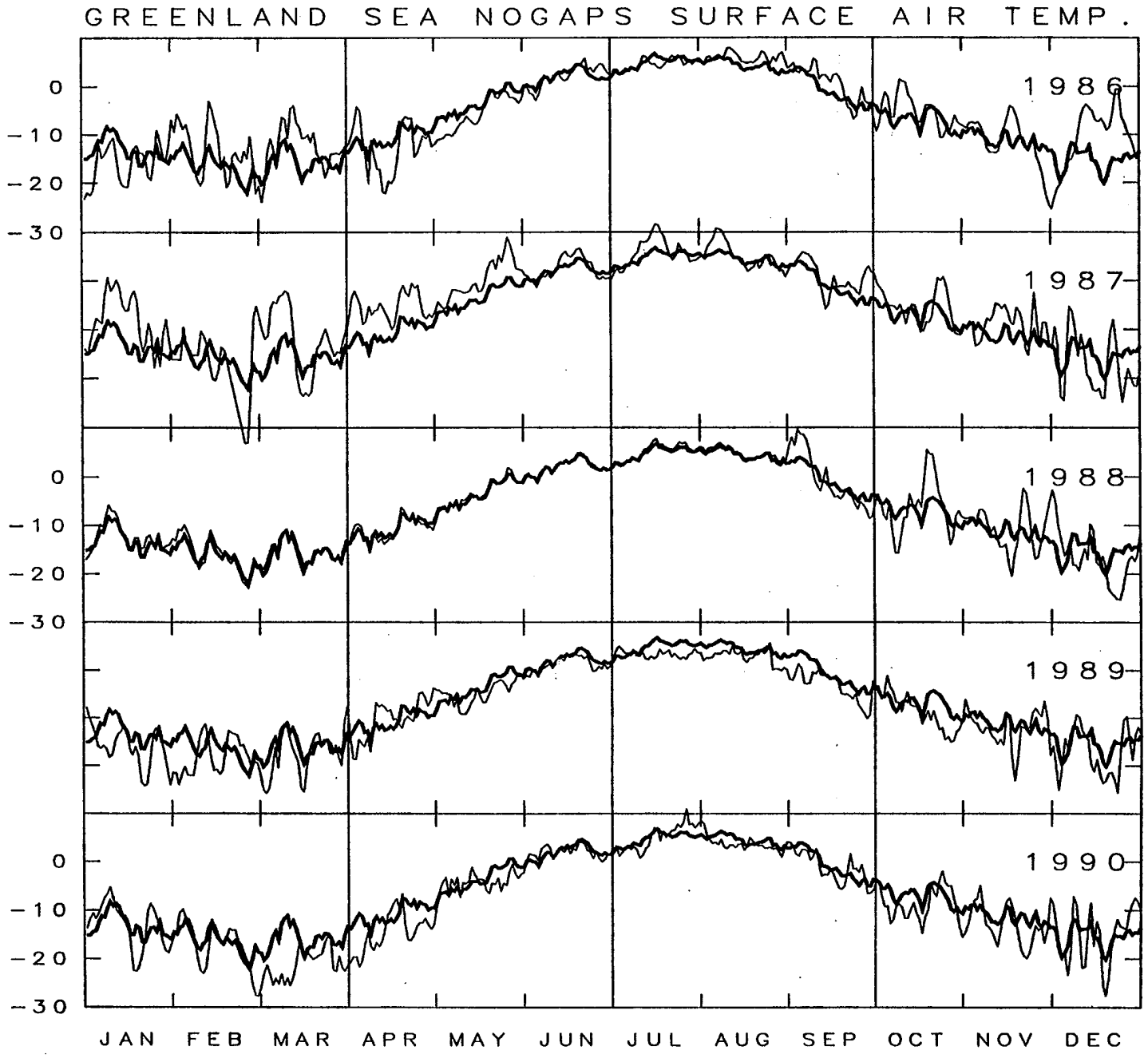
GREENLAND SEA NOGAPS SURFACE AIR TEMP.
1986
1987
1988
1989
1990
0
-10
-20
-30
JAN FEB MAR APR MAY JUN JUL AUG SEP OCT NOV DEC
SURFACE AIR TEMPERATURE (C)

Fig. 3

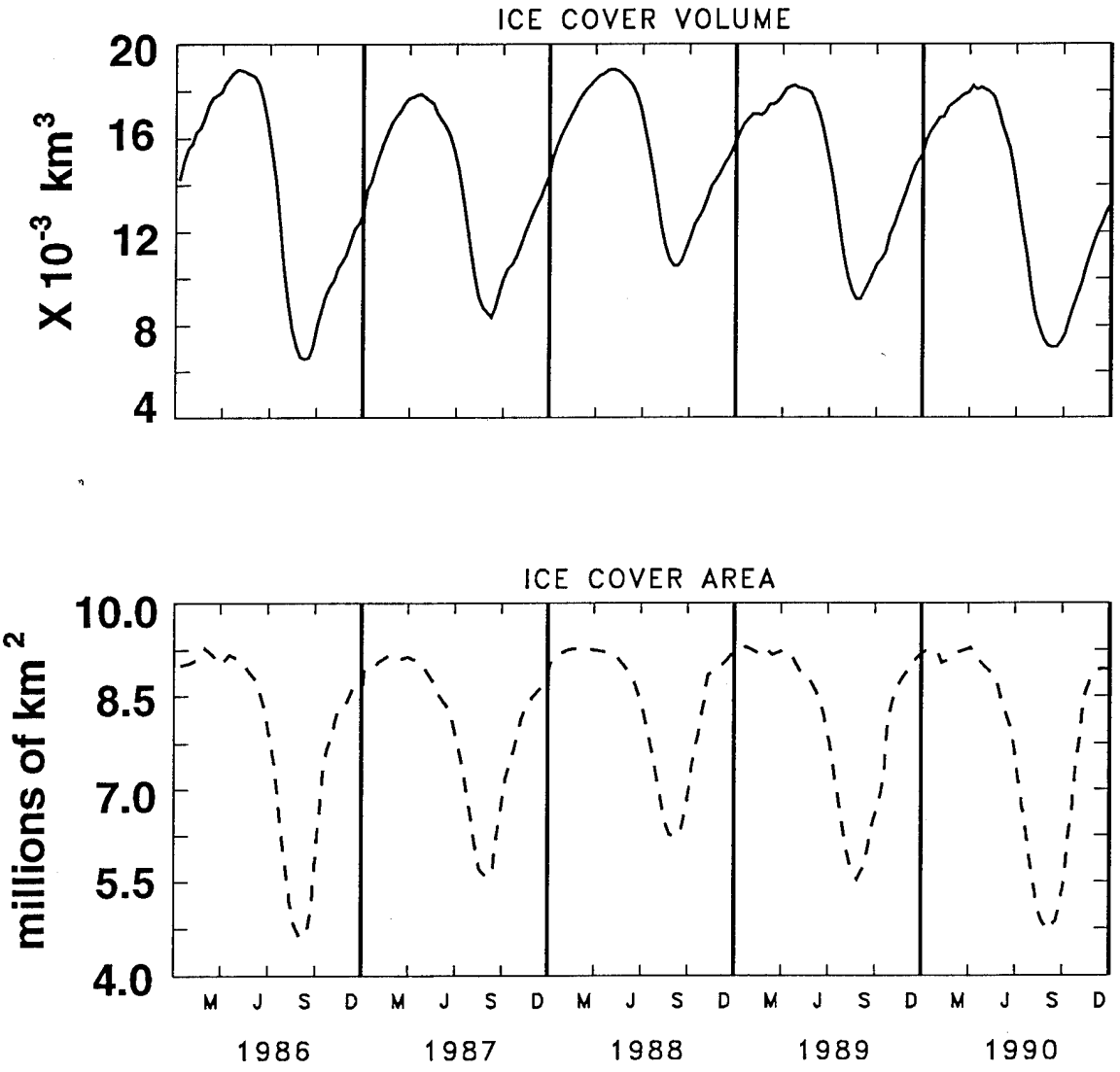
ICE COVER VOLUME
X 10^-3 km^3
20
16
12
8
4
ICE COVER AREA
millions of km^2
10.0
8.5
7.0
5.5
4.0
M J S D M J S D M J S D M J S D M J S D
1986
1987
1988
1989
1990

Fig. 4

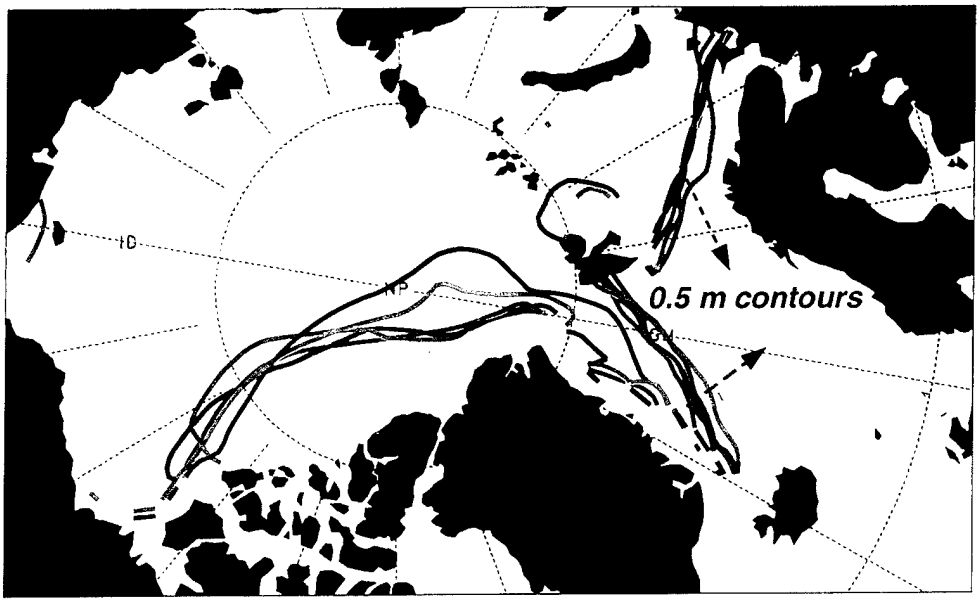

1986 —— 1987 —— 1988

1989 —— 1990

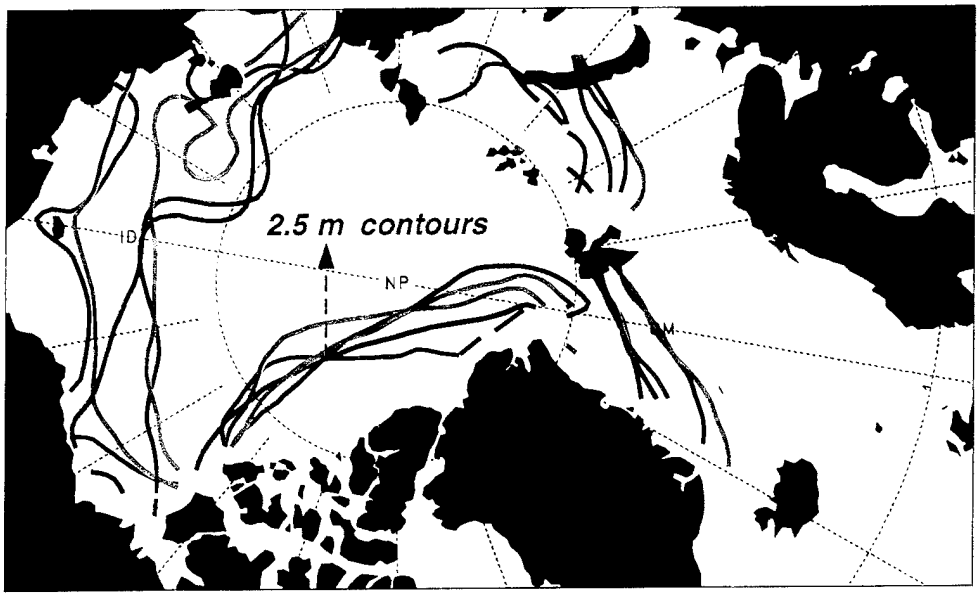

Fig. 5

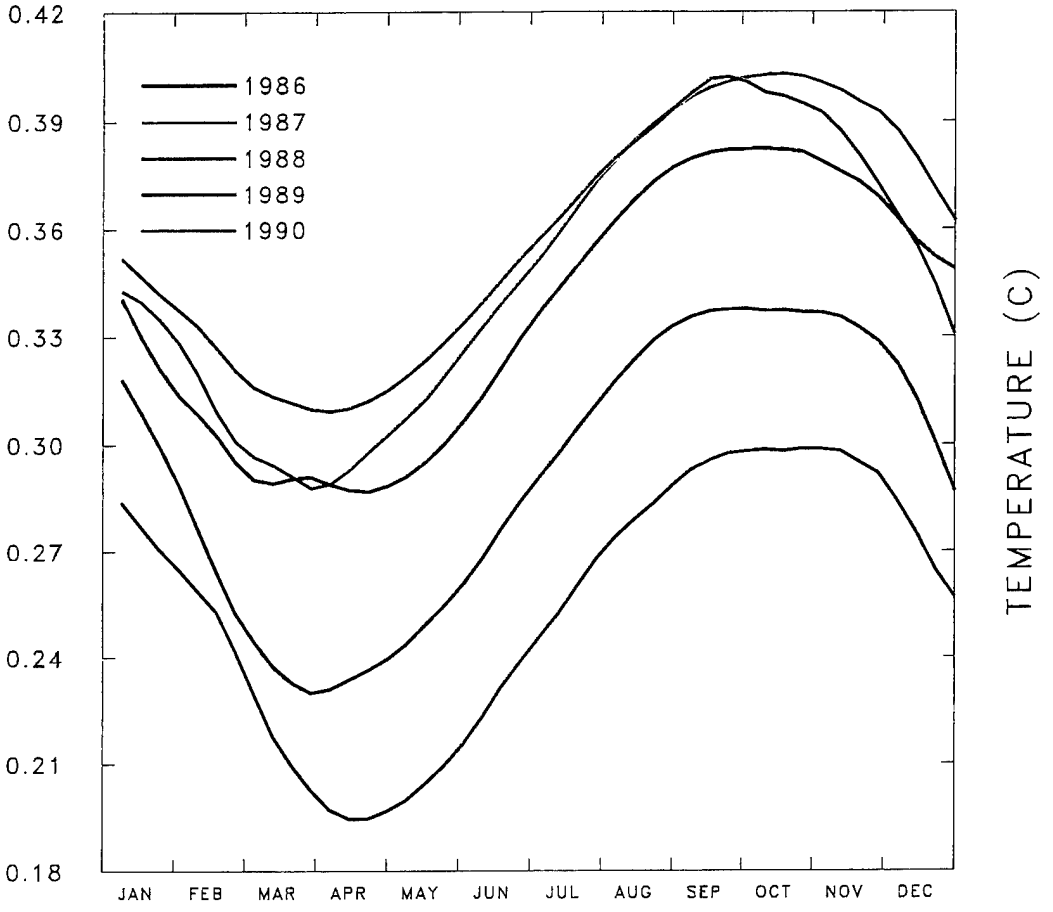
0.42
0.39
0.36
0.33
0.30
0.27
0.24
0.21
0.18
1986
1987
1988
1989
1990
JAN
FEB
MAR
APR
MAY
JUN
JUL
AUG
SEP
OCT
NOV
DEC
TEMPERATURE (C)

Fig. 6

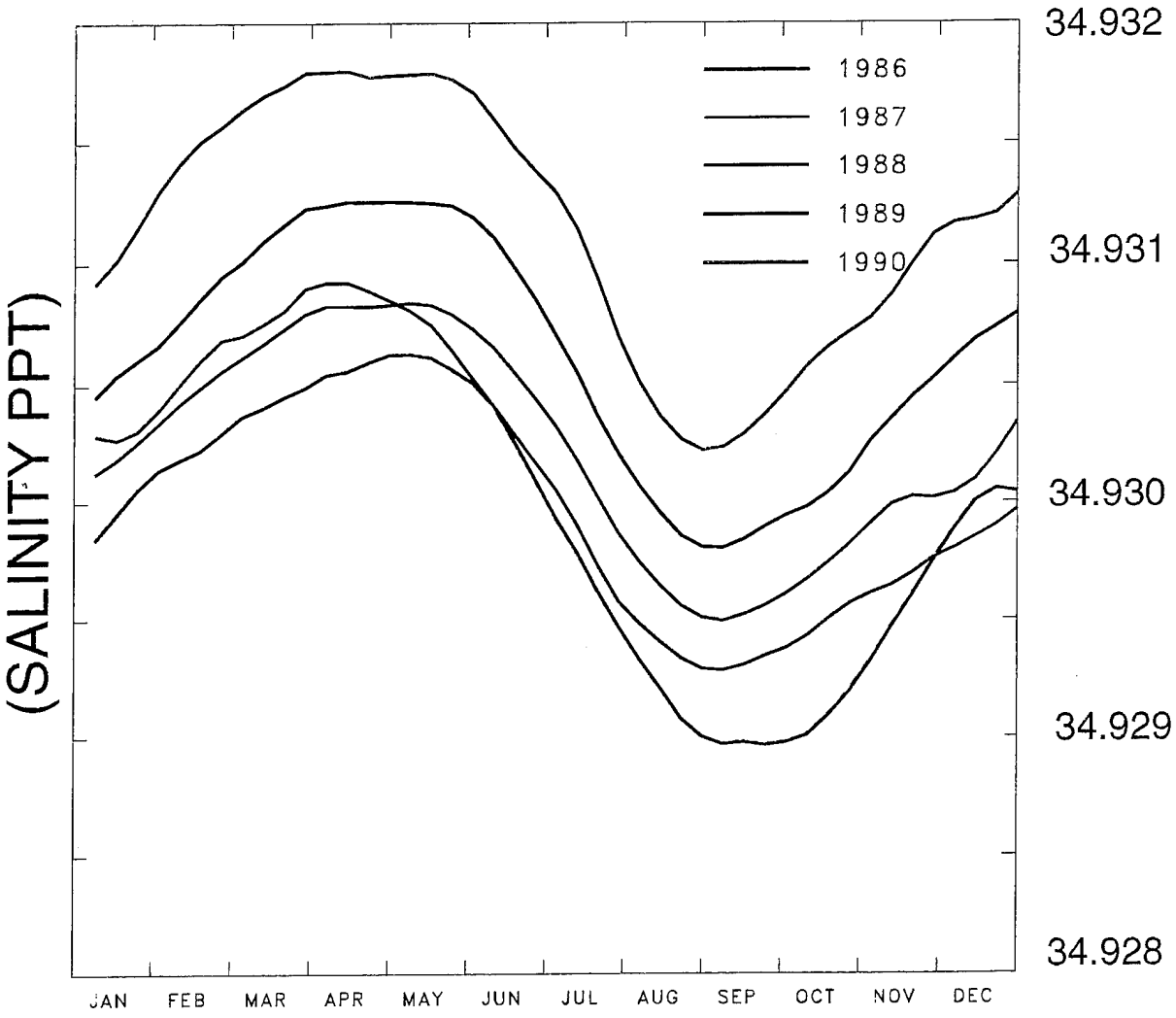
(SALINITY PPT)
34.932
34.931
34.930
34.929
34.928
1986
1987
1988
1989
1990
JAN
FEB
MAR
APR
MAY
JUN
JUL
AUG
SEP
OCT
NOV
DEC

Fig. 7

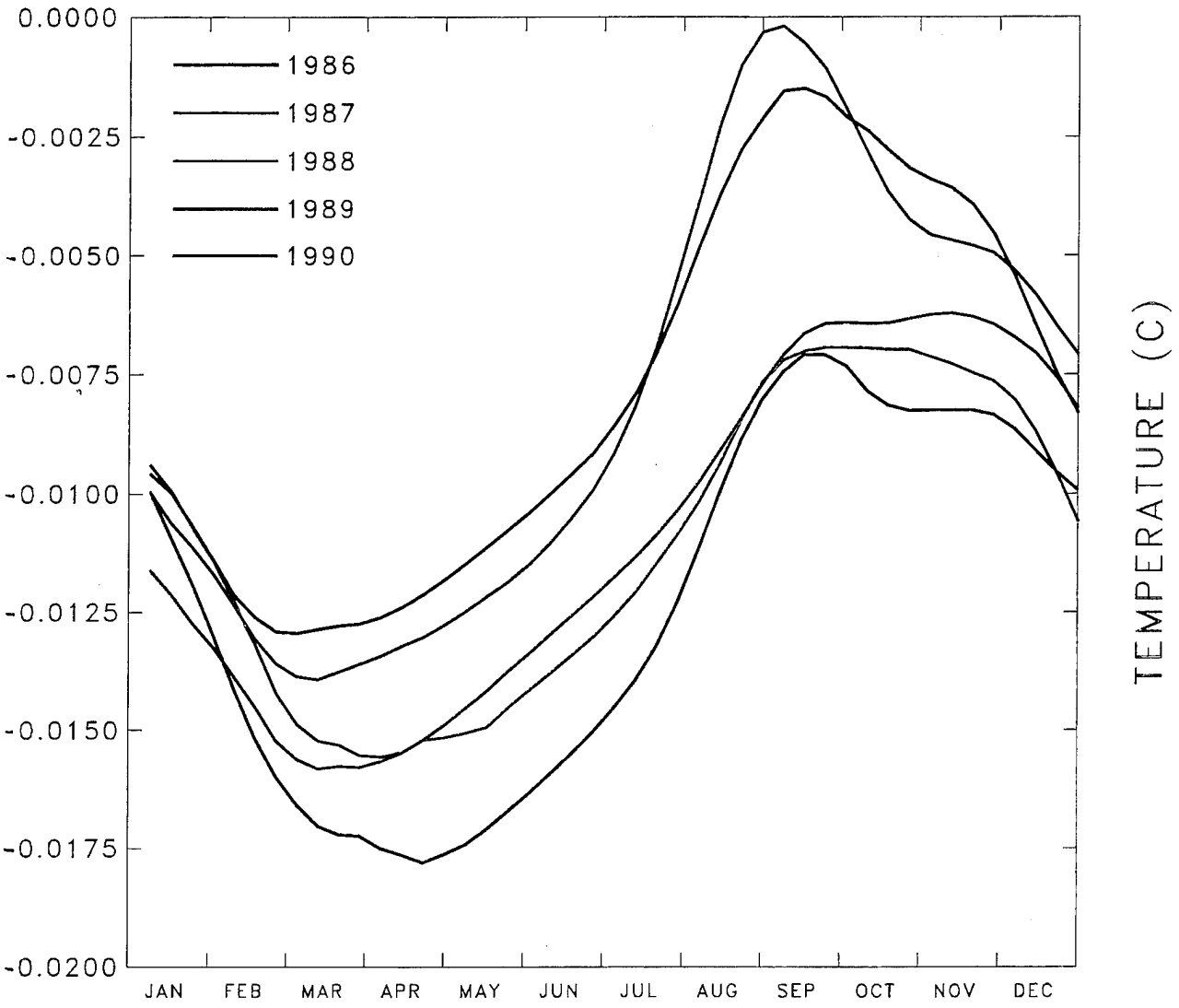
0.0000
-0.0025
-0.0050
-0.0075
-0.0100
-0.0125
-0.0150
-0.0175
-0.0200
1986
1987
1988
1989
1990
JAN
FEB
MAR
APR
MAY
JUN
JUL
AUG
SEP
OCT
NOV
DEC
TEMPERATURE (C)

Fig. 8

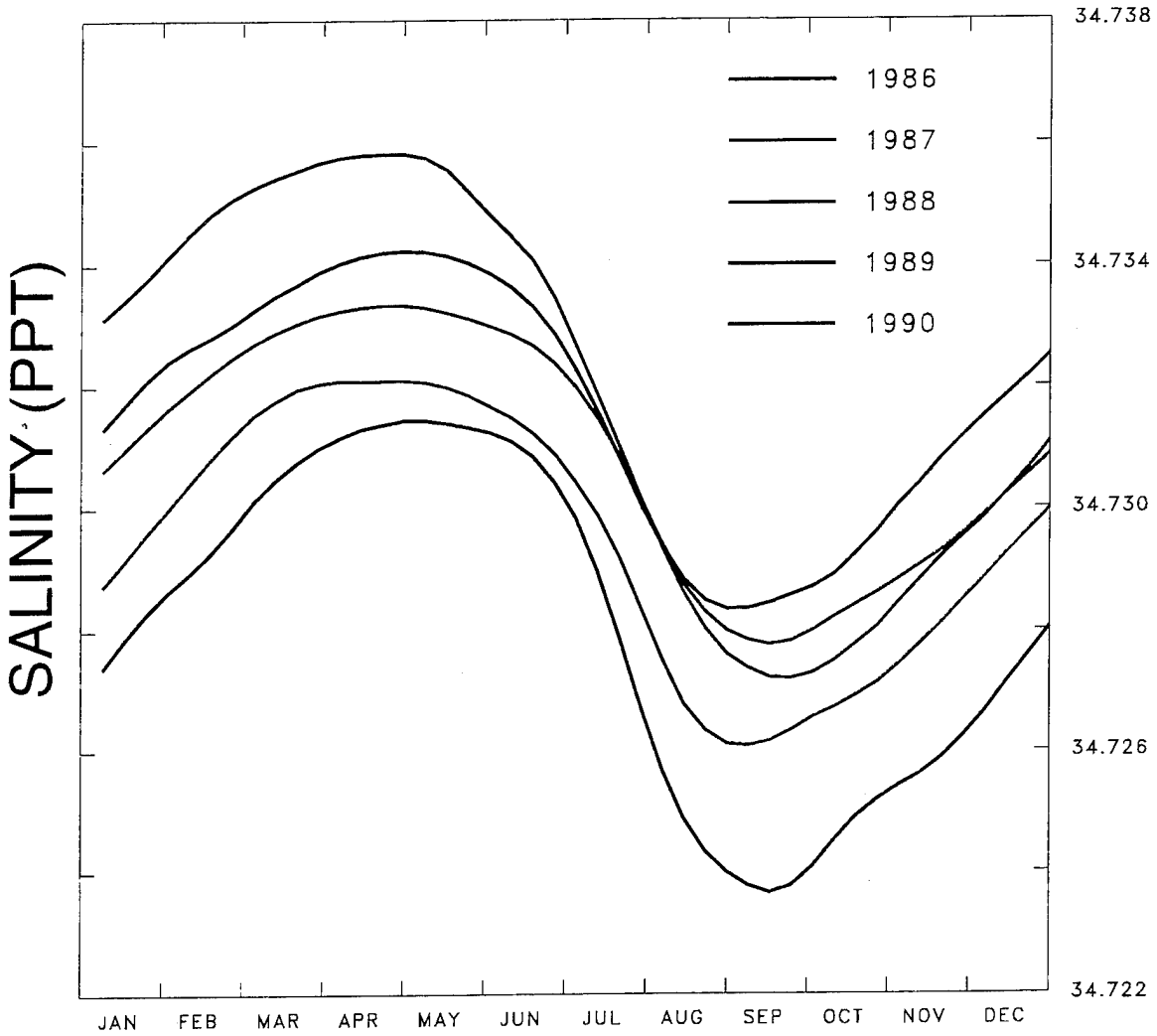
SALINITY (PPT)
34.738
34.734
34.730
34.726
34.722
1986
1987
1988
1989
1990
JAN
FEB
MAR
APR
MAY
JUN
JUL
AUG
SEP
OCT
NOV
DEC

Fig. 9

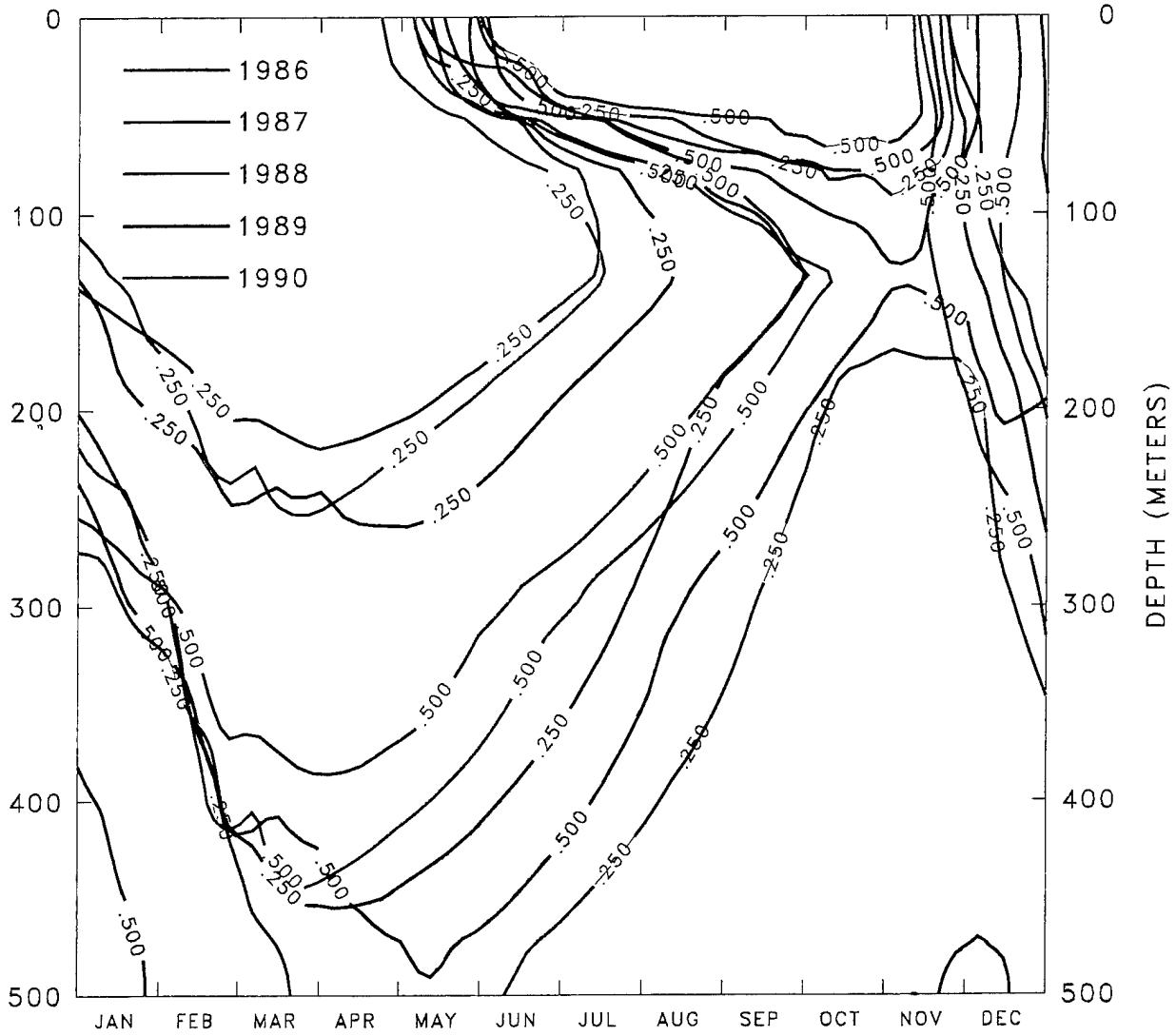
1986
1987
1988
1989
1990
0
100
200
300
400
500
JAN
FEB
MAR
APR
MAY
JUN
JUL
AUG
SEP
OCT
NOV
DEC
DEPTH (METERS)

Fig. 10

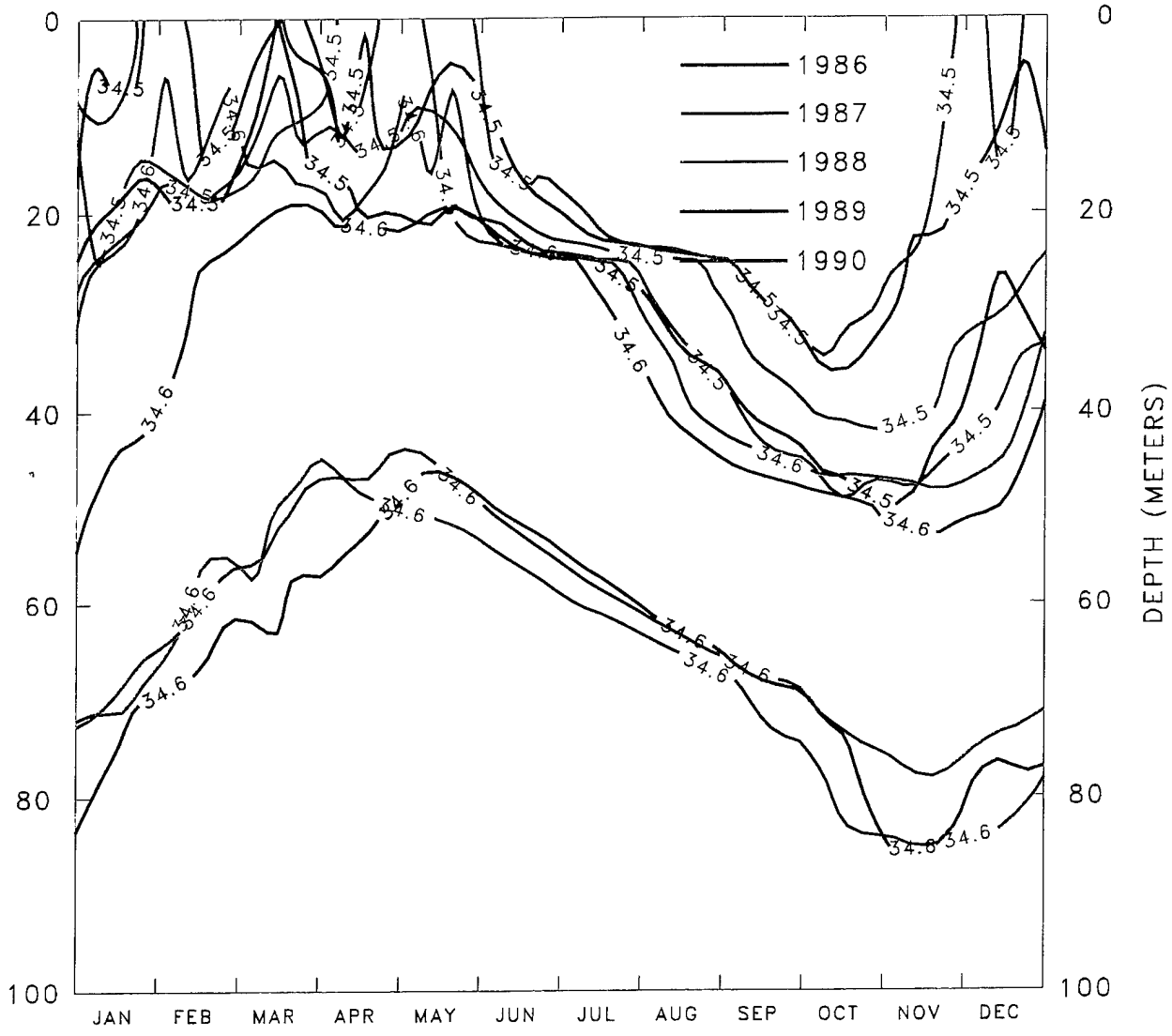
1986
1987
1988
1989
1990
0
20
40
60
80
100
JAN
FEB
MAR
APR
MAY
JUN
JUL
AUG
SEP
OCT
NOV
DEC
DEPTH (METERS)
34.5
34.6

Fig. 11